



Article

Through Diffusion Measurements of Molecules to a Numerical Model for Protein Crystallization in Viscous Polyethylene Glycol Solution

Hiroaki Tanaka ¹, Rei Utata ², Keiko Tsuganezawa ^{2,3}, Sachiko Takahashi ¹ and Akiko Tanaka ^{1,2,3,*}

¹ Confocal Science Inc., Musashino Bld. 5-14-15 Fukasawa, Tokyo 158-0081, Japan; tanakah@confsci.co.jp (H.T.); takahashis@confsci.co.jp (S.T.)

² RIKEN Systems and Structural Biology Center, 1-7-22 Suehiro-cho, Tsurumi, Yokohama 230-0045, Japan; keiko.tsuganezawa@riken.jp (K.T.)

³ RIKEN Center for Biosystems Dynamics Research, 1-7-22 Suehiro-cho, Tsurumi, Yokohama 230-0045, Japan

* Correspondence: aktanaka@a.riken.jp

Abstract: Protein crystallography has become a popular method for biochemists, but obtaining high-quality protein crystals for precise structural analysis and larger ones for neutron analysis requires further technical progress. Many studies have noted the importance of solvent viscosity for the probability of crystal nucleation and for mass transportation; therefore, in this paper, we have reported on experimental results and simulation studies regarding the use of viscous polyethylene glycol (PEG) solvents for protein crystals. We investigated the diffusion rates of proteins, peptides, and small molecules in viscous PEG solvents using fluorescence correlation spectroscopy. In high-molecular-weight PEG solutions (molecular weights: 10,000 and 20,000), solute diffusion showed deviations, with a faster diffusion than that estimated by the Stokes–Einstein equation. We showed that the extent of the deviation depends on the difference between the molecular sizes of the solute and PEG solvent, and succeeded in creating equations to predict diffusion coefficients in viscous PEG solutions. Using these equations, we have developed a new numerical model of 1D diffusion processes of proteins and precipitants in a counter-diffusion chamber during crystallization processes. Examples of the application of anomalous diffusion in counter-diffusion crystallization are shown by the growth of lysozyme crystals.

Keywords: protein crystallization; nucleation; viscosity; diffusion; PEG; FCS; counter-diffusion; self-searching; crystallization scenario



Citation: Tanaka, H.; Utata, R.; Tsuganezawa, K.; Takahashi, S.; Tanaka, A. Through Diffusion Measurements of Molecules to a Numerical Model for Protein Crystallization in Viscous Polyethylene Glycol Solution. *Crystals* **2022**, *12*, 881. <https://doi.org/10.3390/cryst12070881>

Academic Editor: Abel Moreno

Received: 30 May 2022

Accepted: 20 June 2022

Published: 21 June 2022

Publisher's Note: MDPI stays neutral with regard to jurisdictional claims in published maps and institutional affiliations.



Copyright: © 2022 by the authors. Licensee MDPI, Basel, Switzerland. This article is an open access article distributed under the terms and conditions of the Creative Commons Attribution (CC BY) license (<https://creativecommons.org/licenses/by/4.0/>).

1. Introduction

In protein-crystallization studies, polyethylene glycols (PEGs) are one of the main types of precipitants added to protein solutions to reduce their solubility and produce the supersaturation conditions required for the nucleation and growth of crystals. Many protein structures have been determined by growing protein crystals in solutions containing PEGs of various molecular weights (MW) (200–20,000 g/mol) and various concentrations (up to 40 w/v%) as precipitants [1–3]. McPherson and Gavira reported that PEGs with an MW ranging from 2000 to 8000 are the most useful precipitants, and most protein crystals were grown in solutions containing from 4 to 18% PEG for crystallization [1]. These PEG solutions are viscous, and thus may affect the mass transportation, nucleation and growth processes of the protein crystallization. However, only a few papers have experimentally studied the effect of viscosity on protein crystallization [4,5]. Therefore, we precisely measured diffusion rates in viscous solvents and found the advantages of crystallization conditions with pre-mixing viscous high-MW PEGs in the protein solution and diffusing salt as a second component of the precipitant for counter-diffusion crystallization.

Crystallographic technologies are rapidly changing due to the introduction of automation and high-throughput approaches [6,7]; however, it is necessary to reach a supersaturation state for protein crystallization, so that hundreds of crystallization conditions are often tested to allow for a single protein to acquire diffraction-quality crystals. However, some important proteins are difficult to purify in large quantities. Thus, automated microfluidic systems that produce crystals using a counter-diffusion technique have been developed to save the protein sample and obtain good crystals [8]. Counter-diffusion (also known as liquid–liquid diffusion) is a common crystallization method, in which the protein and precipitants are loaded on opposite sides of a tubing chamber and gradually mixed through their diffusion [3,9,10]. In most cases, the protein is loaded into the capillary, the end of which is sealed with a gel plug to keep the protein from flowing out and allow the precipitant to diffuse in from the reservoir. When the precipitant concentration is sufficiently high and the protein chamber is sufficiently long, precipitation and crystallization of the protein occur along the tubing chamber as a result of self-searching for the optimal crystallization scenario [11]. However, in actual experiments, reagent concentrations and the lengths of the tubing chamber have limitations. Therefore, creating an equation that predicts the diffusive mass transport of proteins and precipitants in the system is crucial to optimize the crystallization conditions of counter-diffusion systems [12,13].

The translational diffusion of molecules in solution is described by the well-known Stokes–Einstein (SE) equation:

$$D = k_B T / 6\pi\eta r \quad (1)$$

where k_B is the Boltzmann constant. The diffusion coefficient (D) depends on the hydrodynamic radius of the molecule approximated as a sphere with radius r , temperature T , and solvent viscosity η . According to the SE equation, the diffusion rates of molecules are inversely proportional to the viscosity of the solvent, although, in some macromolecular crowding solvents, such as high-MW PEGs, the measured diffusion coefficient is larger than a value calculated using the macroviscosity of the solution. The phenomena are known as anomalous diffusion [14,15]. We proposed empirical equations to estimate the D value of a protein in a PEG solution from the protein, PEG MWs and concentration of the PEG [16]. Later, Holyst et al. showed that, when considering the viscosity around the molecules (nanoviscosity), the SE equation is correct, even in viscous PEG solutions [17]. Thus, we planned an experimental study of the anomalous effects of PEG solvents on the diffusion rates of small molecules, peptides, and proteins to predict D values in viscous PEG solvents.

We used fluorescence correlation spectroscopy (FCS) to analyze the diffusion phenomenon. FCS is an effective experimental method to observe the translational diffusion of a molecule under various solvent conditions. The original concept of FCS is to detect and analyze the spontaneous fluctuations in the fluorescence emissions of several molecules in a small detection volume caused by thermodynamic fluctuation [18]. The translational diffusion time (τ_D), in which a molecule remains in the focal volume depending on its hydrodynamic radius, and is proportional to the cubic root of its molecular mass for a spherical particle. Experimentally, τ_D is determined by calculating the autocorrelation function from the fluorescence-intensity fluctuations caused by fluorescent molecules diffusing in and out of the detection volume.

According to Holyst et al. [17], the SE equation can be rewritten as Equation (2). If the diffusion constant of the solute in water is assumed to be D_0 and the viscosity of water η_0 , this can be written as:

$$D = k_B T / 6\pi\eta_{nano} r = D_0 \times \eta_0 / \eta_{nano} \quad (2)$$

where D and η_{nano} are the diffusion constant of the solute and the nanoviscosity around the solute molecule in the solvent. The τ_D value of a solute is inversely proportional to D ; therefore, Equation (2) shows the following relation:

$$\tau_D = k_1 / D = k_1 \eta_{nano} / D_0 \eta_0 = k_1 \eta_{nano} \tau_{D0} / \eta_0 = k_2 \tau_{D0} \times \eta_{nano} \quad (3)$$

where k_1 and k_2 are specific constants.

We measured the τ_D values of small molecules, peptides, and proteins in various viscous PEG solvents in this paper. In viscous, high-MW-PEG solutions, the diffusion rates of small molecules are selectively susceptible to anomalous diffusion and not inversely proportional to the viscosity of the solution (macroviscosity). Our previous model [16] is greatly improved in this paper with the use of the newly measured results.

The substantial difference between the diffusions of a small molecule and a protein in PEG solution indicated the following benefits to counter-diffusion crystallization in viscous high-MW-PEG solutions: the delays in the diffusion rates of the various precipitants, such as salts and organic solvents, will be smaller than previously expected, and, at the same time, the protein leakage from the crystallization chamber will be suppressed. We have developed a new numerical model of the 1D diffusion processes of the proteins and precipitants in the counter-diffusion chamber, based on the diffusion times of molecules newly measured in the PEG solutions. The new calculation allows us to point out the advantage of using high-MW PEGs in the counter-diffusion crystallization. We have also demonstrated the advantage with an example of lysozyme crystallization.

2. Materials and Methods

2.1. Materials

PEG1000, PEG3350, PEG6000, PEG10,000, and PEG20,000 were purchased from Hampton Research Chemicals (Aliso Viejo, CA, USA). The fluorescent molecules, TAMRA (MW = 528.0) and ALEXA647 (MW = 1155.1), were purchased from Olympus (Tokyo, Japan). The TAMRA-labeled synthetic peptides, SHP-1 binding peptide (10-mer TAMRA: ITpYSLKGGK-TAMRA, MW = 1572.6) and p53 N-terminal peptide (16-mer TAMRA: SQETFSDLWKLLPEN-K-TAMRA, MW = 2346.6), were purchased from Toray Research Center, Inc. (Tokyo, Japan). Alexa Fluor 647-labelled goat anti-human immunoglobulin G (IgG, MW = 150,000) was purchased from Molecular Probes (Eugene, OR, USA). Egg-white lysozyme was purchased from FUJIFILM (Tokyo, Japan).

2.2. Preparation of the Protein Samples

Human-bromodomain-containing protein 2 (Brd2) (accession: P25440.2, 74aa-194aa, MW = 15,000), and mouse secernin-1 (accession: Q9CZC8.1, 1aa-414aa, MW = 46,300) were synthesized by the *Escherichia coli* cell-free protein-synthesis method [19]. The coding cDNA fragments were amplified by polymerase chain reaction, to add a T7 promoter and histidine affinity tag-encoding sequence to the 5'-region, and a T7 terminator sequence to the 3'-region. These subclones were ligated into the pCR2.1-TOPO vector (Invitrogen, Carlsbad, CA, USA) for cell-free protein expression [19–21].

The proteins produced by the *E. coli* cell-free synthesis system with an N-terminal histidine affinity tag with a TEV cleavage site were purified by a HisTrap HP column (Cytiva, Marlborough, MA, USA). The histidine affinity tag was then removed by incubation with TEV protease at 277 K overnight, and the proteins were further purified by a HisTrap HP column and concentrated [22]. Thus, the final protein samples contained additional amino acid sequences derived from the expression vectors, that is, GSSGSSG for the N terminus and SGPSSG for the C terminus. The molecular weights of the final protein samples were 15,388.5 for Brd2 and 47,317.1 for secernin-1.

2.3. Protein Labeling

The amine side chains of the proteins were randomly labeled with Alexa Fluor 647 mono-functional succinimidyl ester (Molecular Probes, Eugene, OR, USA). The Alexa Fluor 647 fluorophore was covalently attached to the protein by the conjugation protocol of the manufacturer. In brief, 13.7 mM protein was dissolved in 0.1 M Na_2CO_3 (pH 8.3) containing the fluorescent dye, and the mixture was stirred for 1 h at room temperature. The free dye molecules were then removed using BioGel P-30 Fine size-exclusion purification resin (Bio-Rad, Hercules, CA, USA). After the labeling step, absorption spectra indicated

that 1.26 mole Alexa Fluor was contained in 1 mole Brd2 molecules, and 1.12 mole in 1 mole secernin-1 molecules.

2.4. FCS Measurements

The FCS measurements of the solution samples were performed with an MF20 single-molecule fluorescence detection system (Olympus, Tokyo, Japan) using the on-board 543 nm (for TAMRA) or 633 nm (for Alexa Fluor) helium–neon laser at a laser power of 100 μ W for excitation [23,24]. For convenience, the experiments were performed in 384-well glass-bottom plates using a sample volume of 30 μ L.

The fluorescent samples and each PEG solution (*w/v*) were mixed in FCS buffer containing 50 mM Tris/HCl (pH 8.0) and 0.05% Tween 20. Tween 20 was added to suppress glass–surface interactions. The final concentrations of the fluorescent molecules used for the measurements were adjusted to a concentration of 1 nM. All of the FCS measurements were performed in duplicate. The measurement data were obtained with a data acquisition time of 10 s per measurement, and the measurements were performed five times per sample at 296 K. For machine performance verification and normalization of the obtained results, the τ_D values of the standard fluorescent dyes (1 nM TAMRA or 1 nM Alexa Fluor 647) were determined at each measurement. FCS data analysis was performed with the MF20 software package (Olympus). The error bars shown in the graphs represent the standard deviations of five measurements. The Brd2 and secernin-1 samples were purified after fluorescent labelling, although the samples still contained the free-labeling reagent (29% for the Brd2 sample, and 16% for the secernin-1 sample). Therefore, the τ_D values were analyzed by the two-component analysis software of the instrument (MF20) and decomposed into two τ_D values owing to the protein and contaminating free-labeling reagent (Alexa647). For the analysis, the τ_D value of Alexa647 in each PEG solvent was measured and used.

2.5. Viscosity Measurements

Each PEG solution (*w/v%*) containing the FCS buffer was prepared by gentle stirring. The viscosities of the PEG solutions were measured at 296 K by a SV10 sine-wave vibroviscometer (A&D Company, Ltd., Tokyo, Japan) calibrated with JS10 and JS100 calibration solutions (Nippon Grease Co., Ltd., Yokohama, Japan).

2.6. Crystallization

The gel-tube counter-diffusion methods [13,25] were used, as previously mentioned. A capillary (0.47 mm bore) with a gel tube was filled with 7 μ L of a 20% PEG solution (PEG 4000, 10,000, or 20,000) containing 20 mg/mL lysozyme and 50 mM acetate buffer (pH 4.5). The capillaries were vertically placed in a reservoir solution containing 600 mM NaCl, 20% PEG, and 50 mM acetate buffer (pH 4.5) for 30 days at 293 K. Gel tubes with a 1 mm bore were presoaked in each reservoir solution for more than 1 week before sample loading.

2.7. X-ray Diffraction Experiment

The crystals grown in the capillary were picked out and immersed in cryo-protectant solution, including 600 mM NaCl, 40% PEG4000, and 50 mM acetate buffer (pH 4.5) using a cryoloop. They were then flash-frozen with liquid nitrogen.

Data collection was performed using synchrotron radiation at Diamond Light Source beamline i04 equipped with an Eiger2 XE 16M pixel detector. All of the datasets were integrated and scaled using the programs iMosflm [26] and Aimless [27], as implemented in the CCP4 program package [28].

3. Results and Discussion

3.1. Macroviscosity (η_{macro}) of PEG Solutions

The PEG polymers with various MW (1000–20,000) were dissolved in an FCS buffer at 1–20% (*w/v*), and their viscosities were measured (Table 1). The high-MW PEGs (PEG10,000 and PEG20,000) strongly increased the viscosities of the solutions and the lower-MW PEGs

(PEG1000 and PEG3350) were not effective, even at 20%. The measured densities of the solutions were 1.01 g/cm³ (1, 2 and 5%), 1.02 g/cm³ (10%), 1.03 g/cm³ (15%), and 1.04 g/cm³ (20%).

Table 1. Measured macroviscosities of the PEG solutions in the FCS buffer.

MW of PEGs	Viscosity of PEG Solution (mPa·s)					
	Concentrations of PEG Solution * (w/v%)					
	1	2	5	10	15	20
1000	1.25	1.34	1.58	2.13	2.88	4.00
3350	1.33	1.44	1.99	3.53	5.83	8.86
6000	1.45	1.66	2.58	5.05	8.80	15.40
10,000	1.55	1.91	3.28	7.53	14.0	26.00
20,000	1.64	2.28	4.71	12.20	26.90	52.30

* The PEG solutions contained 50 mM Tris-HCl (pH 8.0), and 0.05% Tween 20 for stable FCS measurements.

3.2. Diffusion Times (τ_D) of Compounds, Peptides, and Proteins in Viscous PEG Solutions

The effects of the various PEG solvents (PEG1000, PEG3350, PEG6000, PEG10,000, and PEG20,000 solvents) on the diffusion rates of solute molecules were measured by FCS. We measured the diffusion rates of seven solute molecules: the fluorescence dye TAMRA ($M_w = 528.0$), Alexa647 (1155.1), fluorescence-labeled peptide 10-mer TAMRA (1572.6), and 16-mer TAMRA (2346.6) (Figure 1), fluorescent-labeled proteins, Brd2 (16,500), secernin-1 (48,500), and IgG (150,000) (Figure 2). The Brd2 and secernin-1 samples were purified after fluorescent labelling, although the samples still contained the free-labeling reagent (29% for the Brd2 sample, and 16% for the secernin-1 sample). Therefore, the τ_D values were analyzed by the two-component analysis software of the instrument (MF20) and decomposed into two τ_D values owing to the protein and contaminating free-labeling reagent (Alexa647). For the analysis, the τ_D value of Alexa647 in each PEG solvent was measured and used. The τ_D values of each solute in the various PEG solutions were normalized by their standard τ_D value (τ_{D0}), determined in FCS buffer solution without PEG. The normalized τ_D values are plotted as a function of the macroviscosity of the PEG solution in Figures 1 and 2.

Figures 1 and 2 show that, in the PEG1000 solution, the normalized τ_D values of the seven molecules almost linearly increased with increasing solvent viscosity, which mostly followed the SE equation (Equation (3)). However, the slopes of the regression curves decreased with the increasing MW of the PEGs: PEG1000 (purple) > PEG3350 (blue) > PEG6000 (green) > PEG10,000 (orange) > PEG20,000 (red). In high-MW-PEG solutions, the normalized diffusion mobility was strongly nonlinear and showed considerable deviation to faster diffusion than the SE behavior. The extent of the deviation of normalized τ_D values was more significant when the solute MW was smaller: 16-mer TAMRA (2346.6) < 10-mer TAMRA (1572.6) < Alexa647 (1155.1) < TAMRA (528.0). No clear difference was observed with Brd2 (16.5 k), secernin-1 (48.5 k), and IgG (150 k). These results showed that the extent of diffusion mobility deviations depends on both the MWs of the solute (M_{sol}) and the solvent PEG (M_{peg}). When the M_{sol} is smaller and the M_{peg} is larger, the measured τ_D becomes smaller than expected by the SE equation. Note that the normalized τ_D of the small molecular compounds did not exceed 6-fold, even in 20% PEG20,000 solution with a viscosity of 52.3 mPa·s.

Figure 3 shows the correlations between the normalized solute τ_D and the solvent viscosity, which are shown in Figures 1 and 2, in a double logarithmic plot. The correlations were linearly regressed by the least-squares method and fitted well as the following:

$$\text{Log}(\tau_D/\tau_{D0}) = \text{Log}A + \alpha \text{Log}\eta_{macro}$$

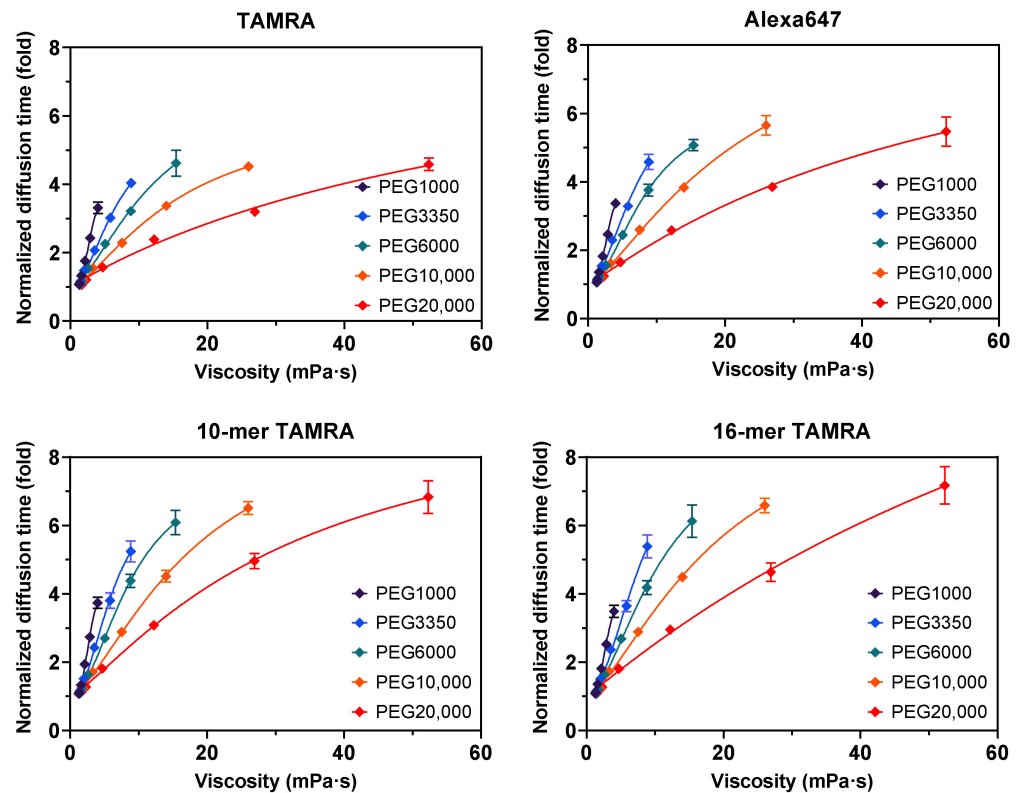


Figure 1. Measured and normalized τ_D values of TAMRA, Alexa647, 10-mer TAMRA, and 16-mer TAMRA in different PEG solvents. The τ_D values were measured and normalized by that measured in FCS buffer solution without PEG. The measurements ($n = 5$) were performed in duplicate. The purple, blue, green, orange, and red points are the results in the PEG1000, PEG3350, PEG6000, PEG10,000, and PEG20,000 solutions, respectively. The data were analyzed and plotted using GraphPad Prism version 8.4.2 for Windows (GraphPad Software, San Diego, CA, USA).

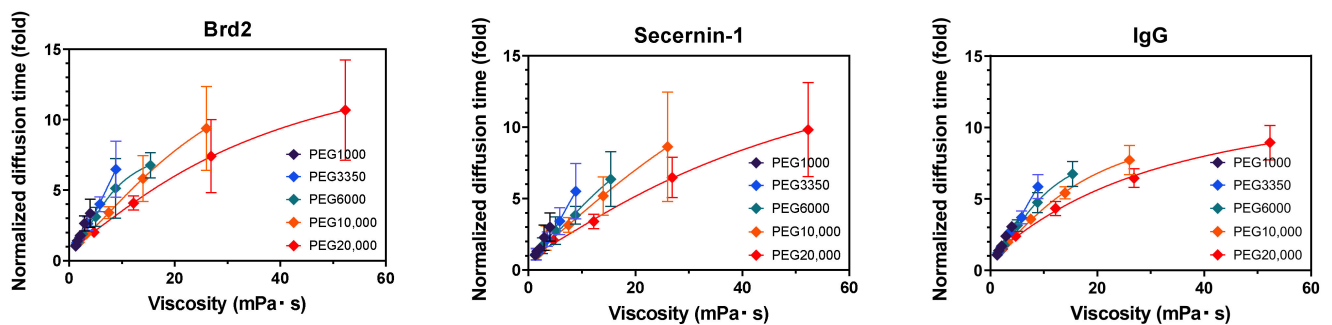


Figure 2. Normalized τ_D values of Brd2, secernin-1, and IgG in different PEG solvents. The measurements ($n = 5$) were performed in duplicate. The measured τ_D values were analyzed by the two-component analysis software of the instrument (MF20) and decomposed into two τ_D values owing to the protein and contaminating free-labeling reagent, then calculated τ_D values of proteins were normalized as in Figure 1.

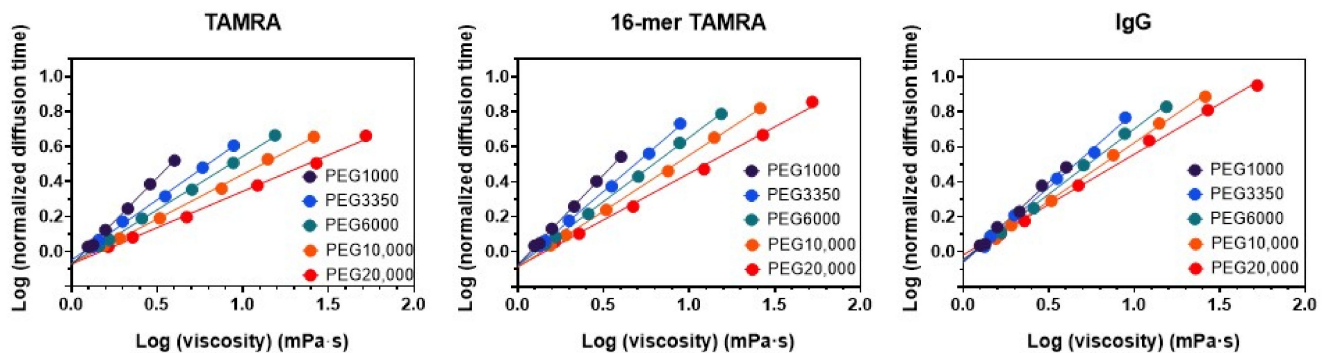


Figure 3. The measured diffusion times (τ_D) depend on macroviscosity (η_{macro}). The relationships between the normalized solute τ_{DS} and solvent η_{macro} s are shown with both logarithmical axes for TAMRA, 16-mer TAMRA and IgG.

By substituting τ_D by referring to Equation (3), this equation is written as Equation (4) with an anomalous index α ($\alpha \leq 1$).

$$\text{Log}(\tau_D/\tau_{D0}) = \text{Log}(k_2\eta_{nano}) = \text{Log}k_2 + \text{Log}\eta_{nano} = \text{Log}k_2 + \alpha\text{Log}\eta_{macro} \quad (4)$$

When SE equation holds α is 1 (Equation (3)), and α would not exceed 1, because the diffusion becomes faster than the SE relation. The estimated α values are 0.9235, 0.6628, 0.5807, 0.5088, 0.4843 and 0.393 for PEG1000, PEG3350, PEG6000, PEG8000, PEG10,000 and PEG20,000, respectively, for TAMRA. 0.9553, 0.7992, 0.6959, 0.6407, 0.6062 and 0.5049 for 16-mer TAMRA and 0.8564, 0.8257, 0.7264, 0.6631, 0.6511 and 0.5699 for IgG. The values of k_2 estimated from Equation (4) are listed in Table 2, (their average value is 0.907).

Table 2. Obtained k_4 , RSP and k_2 values for the solutes.

Solute	M.W.	k_4	RSP	k_2 *
TAMRA	528.0	0.285	0.672	0.91
ALEXA642	1155.1	0.256	1.381	0.91
10-merTAMRA	1572.6	0.236	1.289	0.89
16-mer TAMRA	2346.6	0.213	2.437	0.90
Brd2	16,500.0	0.150	18.460	0.91
secernin-1	48,500.0	0.126	138.800	0.88
ALEXA-IgG	150,000.0	0.142	303.358	0.94

* The average of k_2 is 0.907.

3.3. Quantitative Approximation of the Anomalous Diffusion

It seems plausible that the extent of anomalous diffusion depends on the relative size of the solute molecule and the PEG molecule. Thus, in Figure 4, the anomalous index, α , is plotted against the ratio of the M_{sol} and the M_{peg} , M_{sol}/M_{peg} , with both logarithmic axes. We found that relations of all α and the ratio can be approximated by exponential relations as:

$$\text{Log}(\alpha) = \text{Log}k_3 + k_4\text{Log}\left(\frac{M_{sol}}{M_{peg}}\right) = \text{Log}\left(k_3 \times \left(\frac{M_{sol}}{M_{peg}}\right)^{k_4}\right)$$

$$\alpha = k_3 \times \left(\frac{M_{sol}}{M_{peg}}\right)^{k_4} \quad (5)$$

where k_3 and k_4 are specific constants.

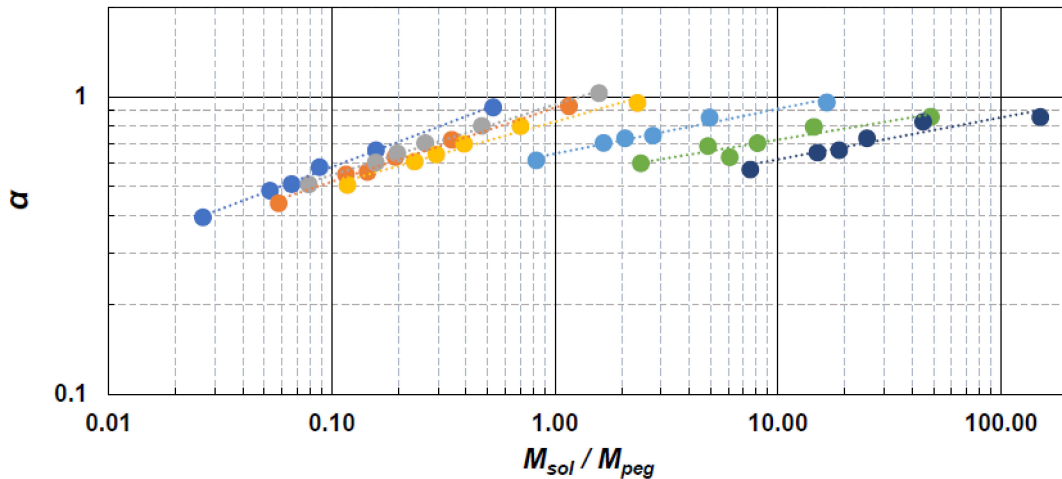


Figure 4. The anomalous index α depends on M_{sol}/M_{peg} . Blue, orange, grey, yellow, light blue, green and dark blue dots correspond to the α value of TAMRA, ALEXA, 10-mer TAMRA, 16-mer TAMRA, Brd2, sesernin-1 and ALEXA-IgG obtained in various molecular weight PEGs, that is PEG1000, PEG3350, PEG6000, PEG8000, PEG10,000 and PEG20,000. Colored dotted lines show exponential approximations for the corresponding dots.

We defined RSP as the ratio of M_{sol} and M_{peg} , where α reaches 1:

$$1 = k_3 \times RSP^{k_4} \quad (6)$$

and Equation (5) can be written as:

$$\alpha = \left(\frac{M_{sol}}{RSP \times M_{peg}} \right)^{k_4} \quad (7)$$

$$\log \alpha = k_4 \log \left(\frac{M_{sol}}{RSP \times M_{peg}} \right) = k_4 \log \left(\frac{1}{RSP} \right) + k_4 \log \left(\frac{M_{sol}}{M_{peg}} \right)$$

Then, k_4 and RSP were determined by calculating the data in Figure 4 using the method of least-squares. They are shown in Table 2.

The obtained k_4 and RSP values are plotted against M_{sol} in Figure 5 with both logarithmic axes. Both parameters can be approximated by exponentiations as follows:

$$\text{Log}k_4 = \text{Log}k_5 - k_6 \text{Log}M_{sol} \quad (8)$$

$$\text{Log}RSP = \text{Log}k_7 + k_8 \text{Log}M_{sol} \quad (9)$$

where k_5 , k_6 , k_7 and k_8 are specific constants. The dotted lines in Figure 5 are the linear regression of the dots, showing that k_5 , k_6 , k_7 and k_8 are 0.6804, 0.1450, 3.819×10^{-4} and 1.1456, respectively. Then, the anomalous index, α in the Equation (7), is as follows, using the estimated values:

$$\alpha = \left(\frac{M_{sol}}{k_7 \times M_{sol}^{k_8} \times M_{peg}} \right)^{k_5 \times M_{sol}^{-k_6}} = \left(\frac{M_{sol}}{3.819 \times 10^{-4} \times M_{sol}^{1.1456} \times M_{peg}} \right)^{0.6804 \times M_{sol}^{-0.145}} \quad (10)$$

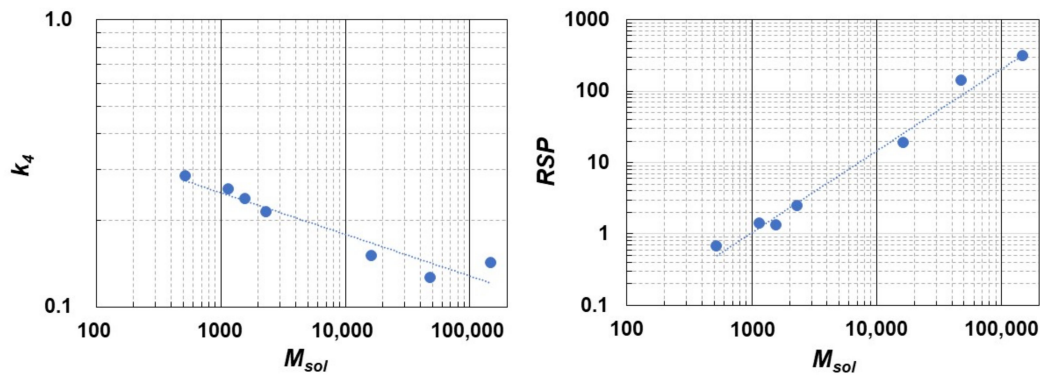


Figure 5. k_4 and RSP values plotted against M_{sol} . Both parameters can be approximated by exponentiation with M_{sol} .

Finally, using Equation (10), we are able to estimate the anomalous index α , so that τ_D of a solute molecule in an arbitrary PEG solvent can be estimated by the following equation.

$$\tau_D / \tau_{D0} = k_2 \times \eta_{macro}^\alpha \quad (11)$$

3.4. Simulation of the Diffusion Processes in the Counter Diffusion Chamber

It is important for counter-diffusion crystallization to estimate the changes over time regarding the concentrations of the protein and crystallization reagents in the counter-diffusion chamber. For the simulation program, we first estimated the macroviscosities of arbitrary MW PEGs with various concentrations. We have reported empirical equations to estimate the values as Equations (1) and (2) in the previous paper [16], so that the results of Table 1 were assigned to the equations, and the parameters were refined by the least-squares methods using the Microsoft Excel solver. The equations with the refined parameters are as follows:

$$\eta_{macro} = 1.002 \times e^{\gamma \times C_{peg}} \quad (12)$$

$$\gamma = 0.045761 \times \ln(M_{peg}) - 0.2554 \quad (13)$$

where C_{peg} is the $w/v\%$ of the PEG solvent. From Equations (12) and (13), η_{macro} of PEG solvents can be calculated from their MWs and concentrations.

The changes in protein and crystallization reagents' concentrations in each area (0.5 mm length) of the counter-diffusion chamber since the start of diffusion can be estimated from each initial concentration by solving the one-dimensional diffusion partial difference equations repetitively by Microsoft Excel macro, as follows:

$$D_{pro}(x, t) = D_{pro0} / \left(0.907 \times \eta_{macro}(M_{peg}, C_{peg}(x, t))^{\alpha(M_{pro}, M_{peg})} \right) \quad (14)$$

$$D_{sol}(x, t) = D_{sol0} / \left(0.907 \times \eta_{macro}(M_{peg}, C_{peg}(x, t))^{\alpha(M_{sol}, M_{peg})} \right) \quad (15)$$

$$\text{if } Ar(x - \Delta x) \leq Ar(x) \text{ then } \beta_1 = \frac{Ar(x - \Delta x)}{Ar(x)} \text{ else } \beta_1 = 1$$

$$\text{if } Ar(x + \Delta x) \leq Ar(x) \text{ then } \beta_2 = \frac{Ar(x + \Delta x)}{Ar(x)} \text{ else } \beta_2 = 1$$

$$C_{pro}(x, t + \Delta t) = C_{pro}(x, t) + \left((C_{pro}(x - \Delta x, t) - C_{pro}(x, t)) \times \beta_1 + (C_{pro}(x + \Delta x, t) - C_{pro}(x, t)) \times \beta_2 \right) \times D_{pro}(x, t) \times \frac{\Delta t}{\Delta x^2} \quad (16)$$

$$C_{sol}(x, t + \Delta t) = C_{sol}(x, t) + \left((C_{sol}(x - \Delta x, t) - C_{sol}(x, t)) \times \beta_1 + (C_{sol}(x + \Delta x, t) - C_{sol}(x, t)) \times \beta_2 \right) \times D_{sol}(x, t) \times \frac{\Delta t}{\Delta x^2} \quad (17)$$

$$C_{peg}(x, t + \Delta t) = C_{peg}(x, t) + \left((C_{peg}(x - \Delta x, t) - C_{sol}(x, t)) \times \beta_1 + (C_{peg}(x - \Delta x, t) - C_{sol}(x, t)) \times \beta_2 \right) \times D_{peg} \times \frac{\Delta t}{\Delta x^2} \quad (18)$$

where D_{pro0} , D_{sol0} and D_{peg} are the diffusion coefficients of the protein, other solute, and PEG in water. $D_{pro}(x, t)$ and $D_{sol}(x, t)$ are the diffusion coefficients of the protein and other solute at position x in the chamber on time t . They are derived from Equations (10)–(13), using $C_{pro}(x, t)$, $C_{sol}(x, t)$ and $C_{peg}(x, t)$ which are the concentrations of the protein, other solute, and PEG at x and on t . $Ar(x)$ is the cross section of the chamber at x . β_1 and β_2 are the cross-section factors. They are determined by the ratio of the two cross sections of adjacent regions having length of Δx (in this case, 0.5 mm). The calculation step time, Δt is 20 s. According to Equations (14) and (15), the diffusion coefficients (D) of molecules (protein, other solute) in the small area at time t are calculated dividing the values in the aqueous solution (D_0) by each calculated ratio, τ_D/τ_{D0} . The τ_D/τ_{D0} of molecules was calculated according to the macroviscosity of the small areas (Equations (10) and (11)), and the value of macroviscosity is determined by concentration and MW of PEG using Equations (12) and (13). The diffusion coefficients of PEG4000, PEG20,000, NaCl, and lysozyme in water are 1.24 [29], 0.476 [29], 15.0 [30], 1.06 [31], $\times 10^{-10}/m^2s^{-1}$, respectively. The counter-diffusion chamber was assumed to be a gel tube with a length of 6 mm and an inner diameter of 1 mm, and a capillary with an inner diameter of 0.5 mm connected to the gel tube, and a protein sample solution was filled with 40 mm in the capillary.

Figure 6 show the results of repetitive calculation of Equations (14)–(18). Figure 6a shows the process of a case where a capillary is filled with 24 mg/mL lysozyme and a crystallization reagent is 20% PEG4000. Figure 6a1 shows the protein concentrations in various areas of the capillary after 4, 32, 64, 128, and 192 days. During this period, the lysozyme diffused out of the capillaries, and its concentration significantly decreased (Figure 6a1). Figure 6a2 shows those of PEG4000. It took time for PEG4000 to diffuse into the capillary. Figure 6a3 plots the PEG4000 concentrations of each part of the capillary on the horizontal axis and the corresponding protein concentrations on the vertical axis. The plotted curves show that the capillary could scan the protein-PEG4000 plane over time, but there is a wide unscanned area in the upper right corner of the figure. Figure 6b shows the case of 20% PEG20,000 with the same lysozyme concentration. Since the diffusion coefficient of PEG20,000 is about 1/3 of that of PEG4000, it took more time to diffuse into the capillary (Figure 6b2). During this period, the lysozyme diffused out of the capillaries, and its concentration significantly decreased (Figure 6b1). As a result, the scanned area of the protein-PEG plane becomes narrower (Figure 6b3). These results show that the self-searching mechanism for the optimal crystallization scenario would not work well when high-MW PEG is used as a precipitant in the counter-diffusion method.

These results indicated that viscous PEG solvents are not good precipitants for counter-diffusion crystallization. On the other hand, high-MW PEG is expected to improve the quality of crystals due to its dehydration effect [32]. Thus, PEG is a reagent that we would like to try.

Regarding the nucleation, the probability is explained by the following equation [33]:

$$\frac{\partial N}{\partial t} = V \times \frac{const}{\eta} \times \exp\left(-\frac{16\pi v^2 \gamma^3}{3(kT)^3 [\ln S]^2}\right) \quad (19)$$

where $\partial N/\partial t$, S , γ , and v , are the nucleation probability, supersaturation, surface energy, and volume of the crystal. V , η and $const$ are the volume of the solution, viscosity and the constant, which are related to the attachment kinetics of growth units. This depends on the molecular charge, the molecular volume, and the density of the solution. Therefore, it is expected that the nucleation probability will decrease in highly viscous solution.

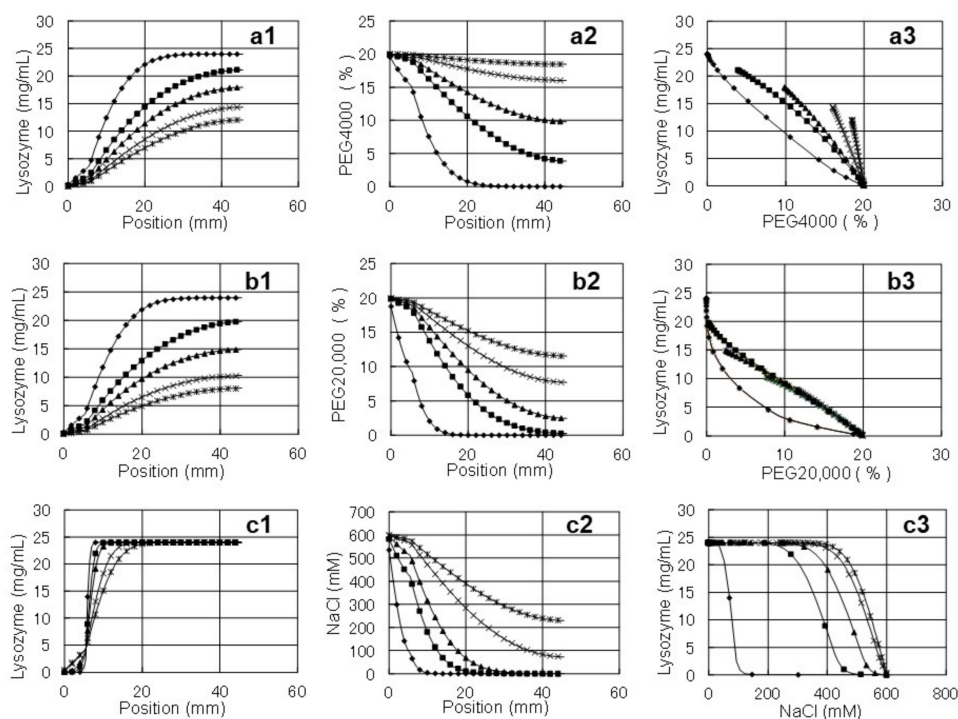


Figure 6. Calculated results of the diffusion processes in the crystallization chamber with 1D simulation. The results of repetitive calculation of Equations (14)–(18) are shown. The crystallization chamber is assumed to be a 6 mm length and 1 mm bore gel tube and 0.5 mm bore glass capillary with a 40 mm length protein solution; (a) 24 mg/mL of lysozyme is loaded into the capillary and 20% of PEG4000 is applied as the precipitant for the reservoir solution; (b) 24 mg/mL of lysozyme and 20% of PEG20,000; (c) 24 mg/mL of lysozyme with 20% of PEG20,000 is loaded into the capillary, 20% of PEG20,000 is presoaked in the gel tube and 20% of PEG20,000 and 600 mM of NaCl is applied as the precipitant for the reservoir solution. The protein concentrations along the chamber are shown in (a1,b1,c1). The abscissa shows the position along the chamber from the open end of the gel tube. The concentrations of the precipitant along the chamber are shown in (a2,b2,c2). The concentration relations of the precipitant and the protein along the chamber are plotted in (a3,b3,c3). For (a,b), \blacklozenge , \blacksquare , \blacktriangle , \times , \times show the values of 4, 32, 64, 128 and 192 days after the starting of the diffusion, respectively. For (c), they show the values of 0.2, 1, 2, 8 and 16 days, respectively. The values are plotted every 2 mm along the chamber.

We reported the nucleation probability in Table 1 of our previous report [34]. The lysozyme was crystallized by batch method with a 50 mM acetate buffer of pH 4.5 and various amounts of PEG4000 and NaCl. The concentrations of NaCl tested were 300, 500, 800 and 1000 mM, and of PEG4000, they were 0, 5, 10, 15, 20 and 25%. The nucleation probability decreased in the higher concentration PEG solvents, almost inversely proportional to the τ_D/τ_{D0} values. The result also suggested the possibility of viscous PEG solvents to obtain fewer but larger crystals.

PEG and small molecules, such as salts, synergistically act on protein crystallization [35]. Therefore, in Figure 6c, we have simulated the following case: a protein sample is pre-mixed with 20% PEG20,000 in advance and crystallization begins upon diffusing 600 mM NaCl contained in 20% PEG20,000 solvent into the capillary. The PEG20,000 concentration was pre-uniform in the counter-diffusion chamber. The concentrations were plotted 0.2, 1, 2, 8 and 16 days after the start of diffusion. The results (Figure 6c3) showed that, after 16 days, most of the protein-NaCl plane was scanned. From these results, it was strongly suggested that crystallization using the counter-diffusion method with high-MW PEG is both possible and promising.

3.5. Quality of Crystals Grown in Viscous PEG Solvents Using Counter-Diffusion Systems

To confirm the crystallization performance obtained by diffusing a small-molecule precipitant into the capillary, where protein samples were pre-mixed with viscous PEG solution in advance, lysozyme crystals were grown in PEG4000, PEG10,000, and PEG20,000 solutions using the counter-diffusion method with gel-tube parts. A lysosome solution with 20 mg protein/mL in each 20% PEG solution containing 50 mM acetate buffer (pH 4.5) was filled in the capillaries and placed in reservoir solutions containing the corresponding 20% PEG, 50 mM acetate buffer (pH 4.5), and 600 mM NaCl at 293 K. After incubation for 20 days at 293 K, crystals were observed in all the capillaries and, after incubation for 30 days, the crystals were harvested. In the X-ray diffraction experiment, three or four crystals grown in each PEG solution were used and the datasets were collected. The crystal-to-detector distance was fixed to the maximum resolution of 1.12 Å. For the crystal from the PEG20,000 solution, an additional dataset with the distance fixed to 1.02 Å was also collected from the same crystal. The dataset from the crystal with the lowest *B* factor of the Wilson plot was selected, and the statistics are listed in Table 3.

Table 3. Data collection and scaling statistics. The values in parentheses are for the highest resolution shells.

	Crystal ID			
	4834BK1	4835M	4836M	4836M *
Major precipitant	PEG4000	PEG10,000	PEG20,000	PEG20,000
Wavelength (Å)	0.8266	0.8266	0.8266	0.7514
Maximum resolution (Å)	1.12	1.12	1.12	1.02
Oscillation range (°)	0.1	0.1	0.1	0.1
Number of images	3600	3600	3600	3600
X-ray exposure time per frame (s)	0.01	0.01	0.01	0.02
Space group	P4 ₃ 2 ₁ 2	P4 ₃ 2 ₁ 2	P4 ₃ 2 ₁ 2	P4 ₃ 2 ₁ 2
Unit-cell parameters (Å)	a = 77.27, b = 77.27, c = 37.55	a = 77.27, b = 77.27, c = 37.83	a = 77.15, b = 77.15, c = 37.62	a = 77.14, b = 77.14, c = 37.62
Resolution range (Å)	54.64–1.12 (1.14–1.12)	54.64–1.12 (1.14–1.12)	54.55–1.12 (1.14–1.12)	54.55–1.02 (1.04–1.02)
No. of observed reflections	1,033,331 (52,069)	1,058,437 (53,038)	1,040,904 (47,802)	1,392,055 (63,330)
No. of unique reflections	43,853 (2159)	44,169 (2164)	43,886 (2064)	58,018 (2687)
Multiplicity	23.6 (24.1)	24.0 (24.5)	23.7 (23.2)	24.0 (23.6)
Completeness (%)	100 (100)	100 (100)	99.8 (96.4)	99.8 (95.5)
$\langle I \rangle / \langle \sigma(I) \rangle$	18.2 (5.8)	27.3 (5.5)	24.6 (7.8)	20.7 (4.1)
R_{merge}	10.0 (57.3)	5.5 (56.7)	8.1 (38.9)	8.3 (78.5)
Wilson <i>B</i> factor (Å ²)	9.2	10.1	8.5	8.4
Overall <i>B</i> factor from relative Wilson plot (Å ²)	−0.34	−0.8	0	0
Mosaicity	0.42 ± 0.11	0.31 ± 0.13	0.17 ± 0.06	0.18 ± 0.06

* The dataset was collected with the proper crystal-to-detector distance, and observed the maximum resolution of 1.02 Å.

The parameters that are usually used to evaluate the protein-crystal quality are the maximum resolution, R_{merge} , $\langle I \rangle / \langle \sigma(I) \rangle$, *B* factor of the Wilson plot, and mosaicity [36,37]. Among these parameters, the maximum resolution, R_{merge} , and $\langle I \rangle / \langle \sigma(I) \rangle$ depend on the experimental diffraction conditions, such as the size of the crystals and intensity of the X-ray. Conversely, the overall *B* factor obtained from the relative Wilson plot is independent of the experimental diffraction conditions [36]. The Wilson *B* factor of the crystal grown in the PEG20,000 solution was the smallest, and the overall *B* factor largest, indicating that the quality of the crystal grown in the solution was better than the others. Regarding the mosaicity, the average value (0.17) and deviation (0.06) were the lowest for the crystal grown in the PEG20,000 solution. The mosaicities of all of the frames are plotted in Figure 7. They showed that the anisotropy was smaller for the crystal grown from the PEG20,000 solution.

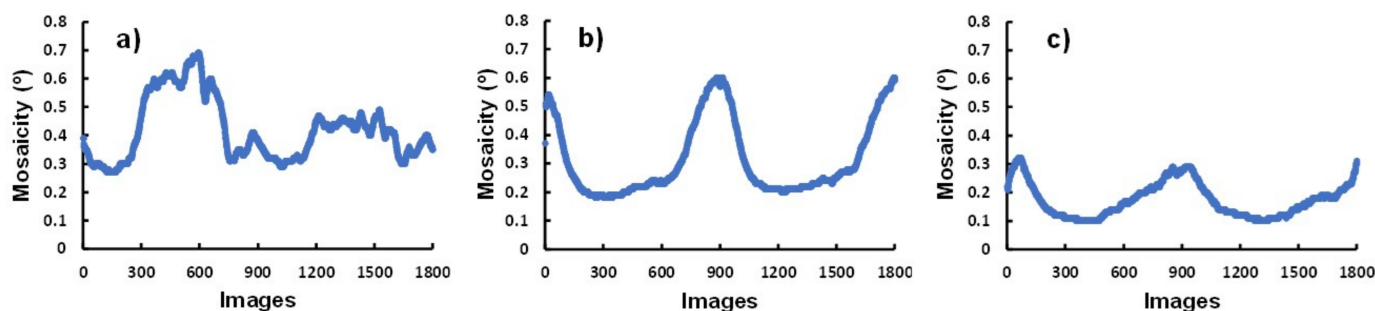


Figure 7. Mosaicities are plotted against the continuous frames: (a) 4834BK1 from PEG4000, (b) 4835M from PEG10,000 and (c) 4836M from PEG20,000.

In this study, lysozyme crystals with good diffractive quality were obtained in the viscous PEG solution using the counter-diffusion method. Their maximum resolutions were comparable to or better than the already registered data for a tetragonal lysozyme crystal in the PDB (for example, PDB ID: 4hp0, 5kxz, 6g8a), except for the crystal grown in space (1iee). Among the three MW PEGs, the best crystals were grown in PEG20,000. There are three possible reasons for this. (1) The density-driven flow around the growing crystals is reduced when the viscosity of the solution is higher. As a result, the highly ordered attachment of the protein molecules to the crystal surface suffers less from the flow [38,39]. (2) In a highly viscous solution, the reduction in the density-driven flow and the decrease of diffusive migration of the protein molecules enhances the formation of the protein depletion zone around the growing crystal [4]. As a result, the protein concentration on the surface of the growing crystal decreases, allowing for good crystals to be grown under lower supersaturation. (3) The excluded volume effect is stronger in high-MW-PEG solutions [40]. This generates a much stronger force to drive the protein molecules onto the crystal surface. The stronger macroscopic force on the surface of the crystal moves the protein molecules closer together inside the crystals and the molecular arrangement in the crystals becomes better. The mechanisms of growing good crystals in viscous high-MW-PEG solutions will be revealed by further investigations.

4. Conclusions

The diffusion mobility of solutes in viscous PEG solvents shows a considerable deviation, which is faster than the expected diffusion rate determined from the macroviscosity. This behavior was quantitatively described in this paper using an approximation model. The model enabled us to describe the mass transportation of molecules during the counter-diffusion crystallization processes. Figure 6a,b clarified that the self-searching mechanism for the optimal crystallization scenario would not work well when high-MW PEG is used as a precipitant in the counter-diffusion method.

However, crystallization in the counter-diffusion chamber containing a uniform concentration of PEG20,000 in advance works well. The greater extent of anomalous diffusion in a high-MW-PEG solution was observed with small-molecule solutes as salt precipitants, so that without a large delay in the crystallization period, the protein solution pre-mixed with viscous high-MW-PEG solutions could be crystallized using salt precipitants in the counter-diffusion crystallization method. Figure 6c shows that the self-searching mechanism worked well under this condition, and most of the protein-NaCl plane could be scanned after 16 days. We further confirmed the possibility of crystallization experiments with lysozyme solution pre-mixed with viscous high-MW PEG.

Author Contributions: Conceptualization, H.T. and A.T.; sample preparation and FCS experiments, R.U., K.T. and A.T.; crystallization experiment, A.T.; validation, A.T.; X-ray structural analysis, S.T. and H.T.; writing—original draft preparation, A.T.; writing—review and editing, A.T. and

H.T.; visualization, A.T. and H.T.; supervision, A.T. and H.T.; project administration, A.T.; funding acquisition, A.T. All authors have read and agreed to the published version of the manuscript.

Funding: This work was supported in part by the Development of Fundamental Technology for Protein Analyses and the Target Protein Research Programs from the Ministry of Education, Culture, Sports, Science and Technology of Japan.

Institutional Review Board Statement: Not applicable.

Informed Consent Statement: Not applicable.

Data Availability Statement: Not applicable.

Acknowledgments: We are grateful to Shigeyuki Yokoyama and Mikako Shirouzu (RIKEN) for their encouraging support.

Conflicts of Interest: The authors declare no conflict of interest.

References

1. McPherson, A.; Gavira, J.A. Introduction to protein crystallization. *Acta Crystallogr. F Struct. Biol. Commun.* **2014**, *70*, 2–20. [[CrossRef](#)] [[PubMed](#)]
2. McPherson, A.; Cudney, B. Optimization of crystallization conditions for biological macromolecules. *Acta Crystallogr. F Struct. Biol. Commun.* **2014**, *70*, 1445–1467. [[CrossRef](#)] [[PubMed](#)]
3. Holcomb, J.; Spellmon, N.; Zhang, Y.; Doughan, M.; Li, C.; Yang, Z. Protein crystallization: Eluding the bottleneck of X-ray crystallography. *AIMS Biophys.* **2017**, *4*, 557–575. [[CrossRef](#)] [[PubMed](#)]
4. Garcia-Ruiza, J.M.; Novella, M.L.; Moreno, R.; Gavira, J.A. Agarose as crystallization media for proteins I: Transport processes. *J. Cryst. Growth* **2001**, *232*, 165–172. [[CrossRef](#)]
5. Gavira, J.A.; Cera-Manjarres, A.; Ortiz, K.; Mendez, J.; Jimenez-Torres, J.A.; Patino-Lopez, L.D.; Torres-Lugo, M. Use of Cross-Linked Poly(ethylene glycol)-Based Hydrogels for Protein Crystallization. *Cryst. Growth Des.* **2014**, *14*, 3239–3248. [[CrossRef](#)]
6. Weber, P.; Pissis, C.; Navaza, R.; Mechaly, A.E.; Saul, F.; Alzari, P.M.; Haouz, A. High-Throughput Crystallization Pipeline at the Crystallography Core Facility of the Institut Pasteur. *Molecules* **2019**, *24*, 4451. [[CrossRef](#)]
7. Lieske, J.; Cerv, M.; Kreida, S.; Komadina, D.; Fischer, J.; Barthelmess, M.; Fischer, P.; Pakendorf, T.; Yefanov, O.; Mariani, V.; et al. On-chip crystallization for serial crystallography experiments and on-chip ligand-binding studies. *IUCr* **2019**, *6*, 714–728. [[CrossRef](#)]
8. De Wijn, R.; Hennig, O.; Roche, J.; Engilberge, S.; Rollet, K.; Fernandez-Millan, P.; Brillet, K.; Betat, H.; Morl, M.; Roussel, A.; et al. A simple and versatile microfluidic device for efficient biomacromolecule crystallization and structural analysis by serial crystallography. *IUCr* **2019**, *6*, 454–464. [[CrossRef](#)]
9. Garcia-Ruiz, J.M.; Moreno, A. Investigations on protein crystal growth by the gel acupuncture method. *Acta Crystallogr. D Struct. Biol. Commun.* **1994**, *D50*, 484–490. [[CrossRef](#)]
10. Hashizume, Y.; Inaka, K.; Furubayashi, N.; Kamo, M.; Takahashi, S.; Tanaka, H. Methods for Obtaining Better Diffractive Protein Crystals: From Sample Evaluation to Space Crystallization. *Crystals* **2020**, *10*, 78. [[CrossRef](#)]
11. Otorola, F.; Garcia-Ruiz, J.M. Computer model of the diffusion/ reaction interplay in the gel acupuncture method. *J. Cryst. Growth* **1996**, *169*, 361–367. [[CrossRef](#)]
12. Garcia-Ruiz, J.M.; Otorola, F.; Garcia-Caballero, A. The role of mass transport in protein crystallization. *Acta Crystallogr. F Struct. Biol. Commun.* **2016**, *72*, 96–104. [[CrossRef](#)]
13. Tanaka, H.; Inaka, K.; Sugiyama, S.; Takahashi, S.; Sano, S.; Sato, M.; Yoshitomi, S. A simplified counter diffusion method combined with a 1D simulation program for optimizing crystallization conditions. *J. Synchrotron Radiat.* **2004**, *11*, 45–48. [[CrossRef](#)]
14. Liu, J.; Wu, S.; Cao, D.; Zhang, L. Effects of pressure on structure and dynamics of model elastomers: A molecular dynamics study. *J. Chem. Phys.* **2008**, *129*, 154905. [[CrossRef](#)]
15. Li, C.; Wang, Y.; Pielak, G.J. Translational and rotational diffusion of a small globular protein under crowded conditions. *J. Phys. Chem. B* **2009**, *113*, 13390–13392. [[CrossRef](#)]
16. Tanaka, H.; Takahashi, S.; Yamanaka, M.; Fukuyama, S.; Sano, S.; Motohara, M.; Kobayashi, T.; Yoshitomi, S.; Tanaka, T. Diffusion Coefficient of the Protein in Various Crystallization Solutions: The Key to Growing High-quality Crystals in Space. *Microgravity Sci. Technol.* **2006**, *18*, 91–94. [[CrossRef](#)]
17. Holyst, R.B.A.; Szymanski, J.; Wilk, A.; Patkowski, A.; Gapinski, J.; Zywockinski, A.; Kalwarczyk, T.; Kalwarczyk, E.; Tabaka, M. Scaling form of viscosity at all length-scales in poly(ethylene glycol) solutions studied by fluorescence correlation spectroscopy and capillary electrophoresis. *Phys. Chem. Chem. Phys.* **2009**, *11*, 9025–9032. [[CrossRef](#)]
18. Haustein, E.; Schwille, P. Fluorescence correlation spectroscopy: Novel variations of an established technique. *Annu. Rev. Biophys. Biomol. Struct.* **2007**, *36*, 151–169. [[CrossRef](#)]
19. Kigawa, T.; Yabuki, T.; Yoshida, Y.; Tsutsui, M.; Ito, Y.; Shibata, T.; Yokoyama, S. Cell-free production and stable-isotope labeling of milligram quantities of proteins. *FEBS Lett.* **1999**, *442*, 15–19. [[CrossRef](#)]

20. Kigawa, T. Cell-free protein production system with the E. coli crude extract for determination of protein folds. *Methods Mol. Biol.* **2010**, *607*, 101–111. [[CrossRef](#)]
21. Kigawa, T.; Yabuki, T.; Matsuda, N.; Matsuda, T.; Nakajima, R.; Tanaka, A.; Yokoyama, S. Preparation of Escherichia coli cell extract for highly productive cell-free protein expression. *J. Struct. Funct. Genom.* **2004**, *5*, 63–68. [[CrossRef](#)] [[PubMed](#)]
22. Nakamura, Y.; Umehara, T.; Nakano, K.; Jang, M.K.; Shirouzu, M.; Morita, S.; Uda-Tochio, H.; Hamana, H.; Terada, T.; Adachi, N.; et al. Crystal structure of the human BRD2 bromodomain: Insights into dimerization and recognition of acetylated histone H4. *J. Biol. Chem.* **2007**, *282*, 4193–4201. [[CrossRef](#)] [[PubMed](#)]
23. Tsuganezawa, K.; Watanabe, H.; Parker, L.; Yuki, H.; Taruya, S.; Nakagawa, Y.; Kamei, D.; Mori, M.; Ogawa, N.; Tomabechi, Y.; et al. A novel Pim-1 kinase inhibitor targeting residues that bind the substrate peptide. *J. Mol. Biol.* **2012**, *417*, 240–252. [[CrossRef](#)]
24. Tsuganezawa, K.; Shinohara, Y.; Ogawa, N.; Tsuboi, S.; Okada, N.; Mori, M.; Yokoyama, S.; Noda, N.N.; Inagaki, F.; Ohsumi, Y.; et al. Two-colored fluorescence correlation spectroscopy screening for LC3-P62 interaction inhibitors. *J. Biomol. Screen.* **2013**, *18*, 1103–1109. [[CrossRef](#)]
25. Yamanaka, M.; Inaka, K.; Furubayashi, N.; Matsushima, M.; Takahashi, S.; Tanaka, H.; Sano, S.; Sato, M.; Kobayashi, T.; Tanaka, T. Optimization of salt concentration in PEG-based crystallization solutions. *J. Synchrotron Radiat.* **2011**, *18*, 84–87. [[CrossRef](#)] [[PubMed](#)]
26. Batty, T.G.; Kontogiannis, L.; Johnson, O.; Powell, H.R.; Leslie, A.G. iMOSFLM: A new graphical interface for diffraction-image processing with MOSFLM. *Acta Crystallogr. D Biol. Crystallogr.* **2011**, *67*, 271–281. [[CrossRef](#)]
27. Evans, P.R.; Murshudov, G.N. How good are my data and what is the resolution? *Acta Crystallogr. D Biol. Crystallogr.* **2013**, *69*, 1204–1214. [[CrossRef](#)]
28. Winn, M.D.; Ballard, C.C.; Cowtan, K.D.; Dodson, E.J.; Emsley, P.; Evans, P.R.; Keegan, R.M.; Krissinel, E.B.; Leslie, A.G.; McCoy, A.; et al. Overview of the CCP4 suite and current developments. *Acta Crystallogr. D Biol. Crystallogr.* **2011**, *67*, 235–242. [[CrossRef](#)]
29. Luo, Z.; Zhang, G. Scaling for sedimentation and diffusion of poly(ethylene glycol) in water. *J. Phys. Chem. B* **2009**, *113*, 12462–12465. [[CrossRef](#)]
30. Vitagliano, V.; Lyons, A. Diffusion coefficients for aqueous solutions of sodium chloride and barium Chloride. *J. Am. Chem. Soc.* **1955**, *78*, 1549–1552. [[CrossRef](#)]
31. Dubin, S.B.; Clark, N.A.; Benedek, G.B. Measurement of the rotational diffusion coefficient of lysozyme by depolarized light scattering: Configuration of lysozyme in solution. *J. Chem. Phys.* **1971**, *54*, 5158. [[CrossRef](#)]
32. Heras, B.; Edeling, M.A.; Byriel, K.A.; Jones, A.; Raina, S.; Martin, J.L. Dehydration converts DsbG crystal diffraction from low to high resolution. *Structure* **2003**, *11*, 139–145. [[CrossRef](#)]
33. Manuel Garcia-Ruiz, J. Nucleation of protein crystals. *J. Struct. Biol.* **2003**, *142*, 22–31. [[CrossRef](#)]
34. Tanigawa, N.T.S.; Yan, B.; Kamo, M.; Furubayashi, N.; Kubota, K.; Inaka, K.; Tanaka, H. Novel Device and Strategy for Growing Large, High-Quality Protein Crystals by Controlling Crystallization Conditions. *Crystals* **2021**, *11*, 1311. [[CrossRef](#)]
35. Majeed, S.; Ofek, G.; Belachew, A.; Huang, C.C.; Zhou, T.; Kwong, P.D. Enhancing protein crystallization through precipitant synergy. *Structure* **2003**, *11*, 1061–1070. [[CrossRef](#)]
36. Arai, S.; Chatake, T.; Suzuki, N.; Mizuno, H.; Niimura, N. More rapid evaluation of biomacromolecular crystals for diffraction experiments. *Acta Crystallogr. D Biol. Crystallogr.* **2004**, *60*, 1032–1039. [[CrossRef](#)]
37. Wuttke, J. Multiple Bragg reflection by a thick mosaic crystal. *Acta Crystallogr. A Found. Adv.* **2014**, *70*, 429–440. [[CrossRef](#)]
38. Vekilov, P.G.; Alexander, J.I.; Rosenberger, F. Nonlinear response of layer growth dynamics in the mixed kinetics-bulk-transport regime. *Phys. Rev. E Stat. Phys. Plasmas Fluids Relat. Interdiscip. Top.* **1996**, *54*, 6650–6660. [[CrossRef](#)]
39. Gliko, O.; Booth, N.A.; Vekilov, P.G. Step bunching in a diffusion-controlled system: Phase-shifting interferometry investigation of ferritin. *Acta Crystallogr. D Biol. Crystallogr.* **2002**, *58*, 1622–1627. [[CrossRef](#)]
40. Bhat, R.; Timasheff, S.N. Steric exclusion is the principal source of the preferential hydration of proteins in the presence of polyethylene glycols. *Protein Sci.* **1992**, *1*, 1133–1143. [[CrossRef](#)]